Bimolecular Electron and Energy Transfer Reactivity of Exchange-Coupled Dinuclear Iron(III) Complexes

Brandon T. Weldon,[†,‡] Daniel E. Wheeler,[†] James P. Kirby,[†] and James K. McCusker*[,†,‡]

Department of Chemistry, University of California at Berkeley, Berkeley, California 94720, and Department of Chemistry, Michigan State University, East Lansing, Michigan 48824

Received June 21, 2001

Bimolecular quenching between photosensitizers and exchange-coupled transition metal complexes has been studied in an effort to experimentally establish a link between Heisenberg spin exchange and chemical reactivity. The acceptors are members of the oxo/hydroxo-biscarboxylato class of dinuclear Fe^{III} compounds, where protonation of the oxo bridge provides a means for modulating the magnitude of spin exchange within the cluster. Photoexcitation of solutions containing Ru^{II} polypyridyl sensitizers and the Fe^{III} complexes results in quenching of emission from the ^{3}MLCT excited state of the Ru^{II} chromophores; nanosecond time-resolved absorption measurements demonstrate that quenching occurs, in part, by electron transfer. Decoupling electron transfer driving force (ΔG_0^{ET}) from changes in the magnitude of spin exchange was achieved by varying the bridging carboxylate to afford a series of complexes of the form $[Fe_2O(H)(O_2CR)_2(Tp)_2]^{n+}$ ($n = 0, 1, 2$). Electrochemical measurements reveal a greater than 500 mV shift in cluster reduction potential across the series (i.e., R = CH_3 to CF_3), whereas variable-temperature magnetic susceptibility measurements demonstrate a corresponding invariance in spin exchange between the metal centers ($J_{oxo} = -119 \pm 4$ cm^{-1} and $J_{hydroxo} = -18 \pm 2$ cm^{-1} for $\mathbf{H} = -2J\mathbf{S}_1\cdot\mathbf{S}_2$). Structural analyses suggest that reorganization energies (λ) associated with electron transfer should be identical for all molecules within a given series (i.e., oxo or hydroxo bridged); likewise $\Delta\lambda$ between the series is expected to be small. A comparison of quenching rates for the two extended series firmly establishes that neither reorganization energy nor electron transfer driving force considerations can account for differences in reactivity between oxo-bridged (large spin exchange) and hydroxo-bridged (small spin exchange) quenchers. Upon consideration of energy transfer contributions, it is determined that reactivity differences between the oxo- and hydroxo-bridged quenchers must lie in the relative rates of Dexter energy transfer and/or electron transfer, with the origin of the latter linked to something other than ΔG_0^{ET} or λ. Finally, the extent to which spin exchange within the dinuclear Fe^{III} quenchers can be identified as the key variable influencing these reactivity patterns is discussed.

Introduction

The study of Heisenberg spin exchange interactions has been an area of active research for many years.[1,2] Early experimental and theoretical work on this subject largely focused on fundamental aspects of the mechanism of spin exchange. This research has led to significant advances in our understanding of the phenomenon and an appreciation of its importance in a range of disciplines.[3−7] Much of the interest as it pertains to inorganic chemistry stems from the number of metalloproteins that have been identified to contain polynuclear transition metal clusters at their active sites.[8,9] The exchange coupling present in these systems (both model complexes and the native proteins) has been examined in terms of characterizing the cluster's electronic structure; however, the extent to which it may influence the chemical properties of such clusters has received far less attention.[10] Several groups have considered the issue of spin exchange and electron transfer from a theoretical perspective. Bertrand and Gayda first examined the effect of exchange interactions on redox potentials of 2Fe−2S ferredoxins.[11] Using a simple effective spin Hamiltonian approach, they suggested that the presence of exchange coupling in a $[Fe_2S_2]^{2+}$ cluster could account for as much as a 100 mV shift in the reduction potential of ferredoxins as compared to single-ion rubredoxins. More recently, Noodleman and co-workers revisited this problem using density functional theory.[12] Although the results of their broken-symmetry analysis differed quantitatively from that of Bertrand and Gayda, a qualitatively similar effect of spin exchange on cluster redox potential was discerned. Bersuker and Borshch[13] have demonstrated a large dependence of the transition frequency of electron transfer on the magnetic

[†] University of California at Berkeley.
[‡] Current address: Department of Chemistry, Michigan State University.

(1) O'Connor, C. J. *Research Frontiers in Magnetochemistry*; World Scientific Publishing Co.: Singapore, 1993.
(2) Kahn, O. *Molecular Magnetism*; VCH Publishers: New York, 1993.
(3) Aubin, S. M. J.; Dilley, N. R.; Pardi, L.; Krzystek, J.; Wemple, M. W.; Brunel, L. C.; Maple, M. B.; Christou, G.; Hendrickson, D. N. *J. Am. Chem. Soc.* **1998**, *120*, 4991−5004.
(4) Kahn, O.; Martinez, C. J. *Science* **1998**, *279*, 44−48.
(5) Anderson, K. K.; Dougherty, D. A. *Adv. Mater.* **1998**, *10*, 688−692.
(6) Papoutsakis, D.; Kirby, J. P.; Jackson, J. E.; Nocera, D. G. *Chem. Euro. J.* **1999**, *5*, 1474−1480.
(7) Nishino, M.; Yoshioka, Y.; Yamaguchi, K. *Chem. Phys. Lett.* **1998**, *297*, 51−59.
(8) Holm, R. H.; Kennepohl, P.; Solomon, E. J. *Chem. Rev.* **1996**, *96*, 2239−2314.
(9) Lippard, S. J.; Berg, J. M. *Principles of Bioinorganic Chemistry*; University Science Books: Mill Valley, 1994.
(10) The excited-state properties of exchange-coupled complexes have been examined to some extent. See: McCarthy, P. J.; Gudel, H. U. *Coord. Chem. Rev.* **1998**, *88*, 69.
(11) Bertrand, P.; Gayda, J.-P. *Biochim. Biophys. Acta* **1982**, *680*, 331.
(12) Mouesca, J. M.; Chen, J.-P.; Noodleman, L.; Bashford, D.; Case, D. A. *J. Am. Chem. Soc.* **1994**, *116*, 11898.
(13) Bersuker, I. B.; Borshch, S. A. *Adv. Chem. Phys.* **1992**, 703.

10.1021/ic010659l CCC: $20.00
Published on Web 11/14/2001

exchange interactions of the system. Girerd and co-workers have considered the possibility of a correlation between electron transfer dynamics and spin exchange in some detail, with particular emphasis being placed on the role of double exchange in mixed-valence systems.[14−16] The most recent work on the subject has been that of Bominaar and co-workers. In an insightful series of papers,[15−20] the roles of Heisenberg−Dirac−van Vleck (HDvV) exchange and double exchange have been examined. The resulting theoretical model and simulations of electron transfer rates in mixed-valence systems suggest pronounced effects on both the driving force and reorganization energies associated with electron transfer in exchange-coupled systems. Much less is known about spin exchange effects on energy transfer, although the spectroscopy of exchange-coupled clusters in doped matrixes has provided some information along these lines.[10] Experimental probes of the connection between chemical reactivity and spin exchange are far more scarce.[21,22] Recent studies by various groups have demonstrated that electron transfer kinetics can be perturbed by the presence of an applied magnetic field:[23,24] modulation of m_s levels by a magnetic field can affect rates of electron transfer through magnetically ordered systems by up to 8 orders of magnitude.[25−27] This provides an excellent illustration of how changes in m_s level energies can impact electron transfer dynamics. In a sense, spin exchange can be thought of as achieving similar energetic effects in zero field.[28]

Although our ultimate goal is to examine the effects of spin exchange on biological systems, their inherent complexity makes it prudent to begin the study of this problem in the context of simpler, more tractable synthetic compounds. Toward this end, we have previously communicated results of photoinduced bimolecular quenching studies involving exchange-coupled complexes.[29] The compounds $Fe_2O(O_2CCH_3)_2(Tp)_2$ and $[Fe_2(OH)(O_2CCH_3)_2(Tp)_2]^+$ (where Tp is hydrotris(pyrazolyl)borate) were chosen for study due to the order-of-magnitude difference in spin exchange that accompanies protonation of the oxo bridge.[30−32] Stern−Volmer plots using these two dimers as potential quenchers of the ^{3}MLCT state of $[Ru(dmb)_3]^{2+}$ (where dmb is 4,4′-dimethyl-2,2′-bipyridine) revealed that (a) both dimers do, in fact, quench emission from the ^{3}MLCT state of $[Ru(dmb)_3]^{2+}$ and (b) there is a significant difference in the bimolecular quenching rates of the oxo- and hydroxo-bridged complexes. Specifically, the quenching rate constant was found to increase from $(2.0 \pm 0.2) \times 10^8$ s^{-1} for $Fe_2O(O_2CCH_3)_2(Tp)_2$ to $(3.7 \pm 0.4) \times 10^9$ s^{-1} for $[Fe_2(OH)(O_2CCH_3)_2(Tp)_2]^+$.[33] Control measurements using $Zn(Tp)_2$ gave no indication of quenching, thus establishing the Fe^{III} dimer core as being responsible for the observed reactivity.[34] In addition, nanosecond time-resolved absorption measurements on the hydroxo-bridged dimer revealed a long-lived transient consistent with the formation of electron transfer photoproducts. However, several aspects of the system are affected by protonation in addition to spin exchange, including the reduction potential of the dimer and its geometric structure. Thus, it was difficult to establish a clear link between the different rates of quenching and the change in Heisenberg spin exchange within the Fe^{III} dimer.

This paper describes our efforts at deconvolving this problem in order to assess the influence of spin exchange on electron and energy transfer. Following a more detailed analysis of our initial observations,[29] we demonstrate herein that variations in the reduction potential of dinuclear Fe^{III} complexes in excess of 500 mV can be achieved through synthetic modifications of the iron carboxylate core. Magnetic susceptibility measurements both in the solid state and in solution confirm that the magnitude of Heisenberg spin coupling is insensitive to these modifications. By combining these compounds with several different photosensitizers, a nearly 900 meV spread in electron transfer driving force (i.e., ΔG_0^{ET}) has been achieved in the limit of constant spin exchange. The combined data reveal that neither ΔG_0^{ET} nor λ can account for the observed reactivity differences between oxo- and hydroxo-bridged Fe^{III} dimers. Rather, possible contributions from Dexter transfer, and ultimately spin coupling, must be considered in order to understand the chemistry observed in these systems.

Experimental Section

General. All reagents were obtained from commercial sources and used without further purification. Potassium hydrotris(1-pyrazolyl)borate (KTp) was prepared by a literature method.[35] Elemental analyses and mass spectra were obtained either through the Analytical Facilities, University of California at Berkeley, or M-H-W Laboratories, Phoenix, AZ. MS measurements used standard ESMS conditions, and all spectra agreed with appropriate simulations.

Oxo-biscarboxylato Complexes. The various $[Fe_2O(O_2CR)_2(Tp)_2]^{n+}$ complexes were all prepared similarly using methods described in detail by Armstrong and Lippard for the R = $-O_2CCH_3$ complex.[30−32] A typical preparation of $Fe_2O(O_2CCH_3)_2(Tp)_2$ (**1**) was as follows: To a rapidly stirring solution containing 1.00 g (2.82 mmol) of $Fe(ClO_4)_3 \cdot 10H_2O$ and 0.579 g (7.05 mmol) of $Na(O_2CCH_3) \cdot 3H_2O$ in 10 mL of H_2O was added 0.470 g (1.85 mmol) of KTp in 40 mL of H_2O. A

(14) Blondin, G.; Girerd, J.-J. *Chem. Rev.* **1990**, *90*, 1359.
(15) Bominaar, E. L.; Borshch, S. A.; Girerd, J. J. *J. Am. Chem. Soc.* **1994**, *116*, 7957−7957.
(16) Borshch, S. A.; Bominaar, E. L.; Blondin, G.; Girerd, J. J. *J. Am. Chem. Soc.* **1993**, *115*, 5155−5168.
(17) Bominaar, E. L.; Achim, C.; Borshch, S. A.; Girerd, J. J.; Munck, E. *Inorg. Chem.* **1997**, *36*, 3689−3701.
(18) Bominaar, E. L.; Hu, Z. G.; Munck, E.; Girerd, J. J.; Borshch, S. A. *J. Am. Chem. Soc.* **1995**, *117*, 6976−6989.
(19) Achim, C.; Bominaar, E. L.; Munck, E. *Biol. Inorg. Chem.* **1998**, *3*, 126−134.
(20) Bominaar, E. L.; Achim, C.; Borshch, S. A. *J. Chem. Phys* **1999**, *110*, 11411.
(21) Monzyk, M. M.; Holwerda, R. A. *Inorg. Chem.* **1992**, *31*, 1969−1971.
(22) Achim, C.; Bominaar, E. L.; Staples, R. J.; Munck, E.; Holm, R. H. *Inorg. Chem.* **2001**, *40*, 4389.
(23) Ferraudi, G. *Inorg. Chem.* **2000**, *39*, 2866, and references therein.
(24) Gilch, P.; Pöllinger-Dammer, F.; Musewald, C.; Michel-Beyerle, M. E.; Steiner, U. E. *Science* **1998**, *281*, 982 and references therein.
(25) Petrov, E. G.; Tolokh, I. S.; Demidenko, A. A.; Gorbach, V. V. *Chem. Phys.* **1995**, *193*, 237.
(26) Petrov, E. G.; Tolokh, I. S.; Gorbach, V. V.; May, V. *Chem. Phys.* **1997**, *220*, 249−260.
(27) Turro, N. J.; Khudyakov, I. V.; Gopidas, K. R. *Chem. Phys.* **1992**, *162*, 131−143.
(28) An important aspect of magnetokinetic effects (MKE) is the polarization inherent to Zeeman splitting. This type of splitting, however, does not occur to the same degree in Heisenberg spin exchange systems in the absence of a magnetic field.
(29) Kirby, J. P.; Weldon, B. T.; McCusker, J. K. *Inorg. Chem.* **1998**, *37*, 3658.
(30) Armstrong, W. H.; Spool, A.; Papaefthymiou, G. C.; Frankel, R. B.; Lippard, S. J. *J. Am. Chem. Soc.* **1984**, *106*, 3653.
(31) Armstrong, W. H.; Lippard, S. J. *J. Am. Chem. Soc.* **1983**, *105*, 4837.
(32) Armstrong, W. H.; Lippard, S. J. *J. Am. Chem. Soc.* **1984**, *106*, 4632.
(33) These rates have now been corrected for diffusion. See Experimental Section for details.
(34) Possible effects due to hydrogen bonding to the oxo/hydroxo bridge were considered through studies in acetonitrile/water mixtures. Quenching data obtained on solutions containing up to 10% H_2O (v/v) were identical within experimental error to those measured in dry CH_3CN for both $Fe_2O(O_2CCH_3)_2(Tp)_2$ and $[Fe_2(OH)(O_2CCH_3)_2(Tp)_2]^+$. In addition, data obtained on $[Fe_2(OD)(O_2CCH_3)_2(Tp)_2]^+$ were likewise indistinguishable from data of the protio form. The effect of the overall charge of the quencher is explicitly accounted for with one of the compounds described herein.
(35) Trofimenko, S. *Inorg. Synth.* **1970**, *12*, 99.

golden-brown precipitate formed immediately; however, the solution was allowed to continue stirring for 10−15 min. After the allotted time the mixture was filtered and washed with excess H_2O, followed by small amounts of cold CH_3CN. The resulting green solid was recrystallized from hot CH_3CN. The crystals were then crushed and dried in vacuo. Anal. Calcd for $Fe_2O(O_2CCH_3)_2(Tp)_2$ ($Fe_2C_{22}H_{26}B_2N_{12}O_5$) (**1**): C, 39.32; H, 3.91; N, 25.02. Found: C, 39.34; H, 4.10; N, 25.29. Electronic absorption spectrum (in CH_3CN at 298 K) λ, nm (ϵ, M^{-1} cm^{-1}): 340 (9300), 370 (7600), 460 (970), 492 (900), 700 (140).

$Fe_2O(O_2CCH_2F)_2(Tp)_2$ (2). Substitution of $Na(O_2CCH_3)$ with $Na(O_2CCH_2F)$ in the above preparation gives **2**. Anal. Calcd for $Fe_2O(O_2CCH_2F)_2(Tp)_2 \cdot 3CH_3CN$ ($Fe_2C_{28}H_{33}B_2N_{13}F_2O_5$) (**2**): C, 40.46; H, 4.01; N, 25.29. Found: C, 40.62; H, 3.99; N, 25.37. Electronic absorption spectrum (in CH_3CN at 298 K) λ, nm (ϵ, M^{-1} cm^{-1}): 340 (10 200), 364 (8800), 462 (960), 490 (880), 696 (120).

$Fe_2O(O_2CCH_2Cl)_2(Tp)_2$ (3). Substitution of $Na(O_2CCH_3)$ with $Na(O_2CCH_2Cl)$ in the above preparation gives **3**. Anal. Calcd for $Fe_2O(O_2CCH_2Cl)_2(Tp)_2 \cdot 1.5CH_3CN$ ($Fe_2C_{25}H_{28.5}B_2N_{13.5}Cl_2O_5$) (**3**): C, 37.41; H, 3.59; N, 23.57. Found: C, 37.21; H, 3.84; N, 23.31. Electronic absorption spectrum (in CH_3CN at 298 K) λ, nm (ϵ, M^{-1} cm^{-1}): 338 (10 300), 360 (8900), 464 (960), 490 (890), 698 (130).

$Fe_2O(O_2CCHCl_2)_2(Tp)_2$ (4). Substitution of $Na(O_2CCH_3)$ with $Na(O_2CCHCl_2)$ in the above preparation gives **4**. Anal. Calcd for $Fe_2O(O_2CCHCl_2)_2(Tp)_2$ ($Fe_2C_{22}H_{22}B_2N_{12}Cl_4O_5$) (**4**): C, 32.64; H, 2.74; N, 20.76. Found: C, 33.00; H, 2.79; N, 20.42. Electronic absorption spectrum (in CH_3CN at 298 K) λ, nm (ϵ, M^{-1} cm^{-1}): 338 (10 400), 362 (9400), 468 (940), 490 (880), 690 (130).

$Fe_2O(O_2CCF_3)_2(Tp)_2$ (5). Substitution of $Na(O_2CCH_3)$ with $Na(O_2CCF_3)$ in the above preparation gives **5**. Anal. Calcd for $Fe_2O(O_2CCF_3)_2(Tp)_2$ ($Fe_2C_{22}H_{20}B_2N_{12}F_6O_5$) (**5**): C, 33.81; H, 2.58; N, 21.51. Found: C, 34.10; H, 2.75; N, 21.55. Electronic absorption spectrum (in CH_3CN at 298 K) λ, nm (ϵ, M^{-1} cm^{-1}): 338 (10 800), 370 (10 800), 466 (950), 490 (880), 684 (120).

$Fe_2O(O_2CCH_2OCH_3)_2(Tp)_2$ (6). Substitution of $Na(O_2CCH_3)$ with $HO_2CCH_2OCH_3$ (deprotonated with KOH) in the above preparation gives **6**. Anal. Calcd. for $Fe_2O(O_2CCH_2OCH_3)_2(Tp)_2 \cdot 1.5H_2O$ ($Fe_2C_{24}H_{33}B_2N_{12}O_{8.5}$) (**6**): C, 37.98; H, 4.39; N, 22.15. Found: C, 38.06; H, 4.29; N, 22.25. Electronic absorption spectrum (in CH_3CN at 298 K) λ, nm (ϵ, M^{-1} cm^{-1}): 342 (9200), 370 (7800), 464 (960), 492 (890), 696 (140).

$[Fe_2O(O_2CCH_2N(CH_3)_3)_2(Tp)_2](ClO4)_2$ (7). Substitution of $Na(O_2CCH_3)$ with $O_2CCH_2N(CH_3)_3$ in the above preparation gives **7**. Anal. Calcd for $[Fe_2O(O_2CCH_2N(CH_3)_3)_2(Tp)_2](ClO_4)_2$ ($Fe_2C_{28}H_{42}B_2N_{14}O_{13}Cl_2$) (**7**): C, 34.07; H, 4.30; N, 19.87. Found: C, 33.87; H, 4.56; N, 19.68. Electronic absorption spectrum (in CH_3CN at 298 K) λ, nm (ϵ, M^{-1} cm^{-1}): 340 (9000), 364 (8400), 454 (1100), 490 (890), 688 (120).

Hydroxo-biscarboxylato Complexes. The various $[Fe_2(OH)(O_2CR)_2(Tp)_2]^{n+}$ complexes were all prepared similarly using methods described in detail by Armstrong and Lippard for the $R = -O_2CCH_3$ complex.[30−32] A typical preparation of $[Fe_2(OH)(O_2CCH_3)_2(Tp)_2](ClO_4)$ (**8**) is as follows: To a solution containing 0.100 g (0.149 mmol) of $Fe_2O(O_2CCH_3)_2(Tp)_2$ in 50 mL of diethyl ether, 1 equiv of 0.25 M $HClO_4$ was added. A yellow-brown precipitate formed, which was then filtered, washed with diethyl ether, and then dried in vacuo. Recrystallization was carried out by diethyl ether diffusion into either acetone or methylene chloride solution. Filtration afforded yellow-red needles. Anal. Calcd. for $[Fe_2(OH)(O_2CCH_3)_2(Tp)_2](ClO_4) \cdot 0.5CH_2Cl_2$ ($Fe_2C_{22.5}H_{28}B_2N_{12}Cl_2O_9$) (**8**): C, 33.17; H, 3.46; N, 20.63. Found: C, 32.93; H, 3.70; N, 20.40. Electronic absorption spectrum (in CH_3CN at 298 K) λ, nm (ϵ, M^{-1} cm^{-1}): 364 (8900).

$[Fe_2(OH)(O_2CCH_2F)_2(Tp)_2](ClO_4)$ (9). Substitution of $Fe_2O(O_2CCH_3)_2(Tp)_2$ with $Fe_2O(O_2CCH_2F)_2(Tp)_2$ in the above preparation gives **9**. Anal. Calcd for $[Fe_2(OH)(O_2CCH_2F)_2(Tp)_2](ClO_4) \cdot 2(CH_3)_2CO$ ($Fe_2C_{28}H_{39}B_2N_{12}ClO_{11}$) (**9**): C, 36.37; H, 4.04; N, 18.18. Found: C, 36.06; H, 3.89; N, 18.59. Electronic absorption spectrum (in CH_3CN at 298 K) λ, nm (ϵ, M^{-1} cm^{-1}): 374 (6700).

$[Fe_2(OH)(O_2CCH_2Cl)_2(Tp)_2](ClO_4)$ (10). Substitution of $Fe_2O(O_2CCH_3)_2(Tp)_2$ with $Fe_2O(O_2CCH_2Cl)_2(Tp)_2$ in the above preparation gives **10**. Anal. Calcd for $[Fe_2(OH)(O_2CCH_2Cl)_2(Tp)_2](ClO_4) \cdot (CH_3)_2CO$ ($Fe_2C_{25}H_{31}B_2N_{12}Cl_3O_{10}$) (**10**): C, 33.40; H, 3.50; N, 18.69. Found: C, 33.60; H, 3.74; N, 18.54. Electronic absorption spectrum (in CH_3CN at 298 K) λ, nm (ϵ, M^{-1} cm^{-1}): 374 (7800).

Physical Measurements: Cyclic Voltammetry. Electrochemical measurements were carried out in an argon-filled drybox (Vacuum Atmospheres) using a BAS CV-50W electrochemical analyzer with a Pt working electrode and a $Ag/AgNO_3$ reference electrode. Compounds were dissolved in CH_3CN (distilled over CaH_2) that was 0.1 M in NBu_4PF_6. All measurements were made on solutions containing trace amounts of ferrocene to allow for internal calibration of the observed reduction potential.

Variable-Temperature Magnetic Susceptibility. Magnetic susceptibility data were collected using a Quantum Design MPMS SQUID magnetometer interfaced to an IBM PC. A finely ground sample of each compound was packed into a cylindrical Kel-F sample container. Data were collected in an applied field of 25.00 kG. Following each temperature change, the system was kept at the new temperature for an additional 10 min before data collection to ensure thermal equilibration of the sample. Data were corrected for diamagnetism using Pascal's constants[36] and reported herein as effective magnetic moments. Solution susceptibility measurements at room temperature were made via the Evans NMR method[37] using a Bruker 300 MHz spectrometer.

Electronic Absorption and Emission Measurements. All spectroscopic data were obtained on samples dissolved CH_3CN that had been distilled over CaH_2 and stored under an inert atmosphere. Static electronic absorption spectra were recorded using a Hewlett-Packard 8452A diode array spectrophotometer. Static emission spectra were acquired using a Spex FluoroMax fluorimeter as described elsewhere.[38]

Samples for Stern−Volmer quenching experiments using Ru^{II} polypyridyl complexes as sensitizers and the oxo/hydroxo Fe^{III} dimers as quenchers were prepared in a Vacuum Atmospheres glovebox. A stock solution of sensitizer ($\sim 10^{-6}$ M) and tetrabutylammonium hexafluorophosphate ($\sim$0.075 M) was prepared from dry, degassed acetonitrile. From this was prepared a quencher stock solution ($\sim$2.00 mM). Samples with varying quencher concentrations where then prepared using standard volumetric techniques. In sealable test tubes the volumetric ratio of sensitizer to quencher stock solutions was controlled with a pipetman (100−1000 μL). Typically quencher volumetric dilution ratios of 0.1/5.1, 0.1/2.1, 0.25/2.25, 0.5/2.5, 1/3, and 1/2 were employed with this technique. The sample tubes where then sealed and removed from the glovebox for immediate emission lifetime measurements.

Nanosecond time-resolved emission and absorption data were collected using a Nd:YAG-pumped OPO spectrometer that has been described previously.[38] Emission was monitored at 620 nm. All time-resolved measurements were recorded following 450 nm excitation, except for compounds **4**, **6**, and **10**, for which data were collected following excitation at 532 nm. Bimolecular quenching rates were corrected for diffusion. Following Clark and Hoffman,[39,40] the quenching rate k_q' can be obtained from

$$\frac{1}{k_q} - \frac{1}{k_d} = \frac{1}{K_D k_q'} \qquad (1)$$

where K_D is the equilibrium constant and k_q is the measured bimolecular quenching constant.[41] Expressions for k_d are based on the Debye−Smoluchowski and Eigen equations and can be found elsewhere.[39,40] Radii for the Ru^{II} and dinuclear Fe^{III} compounds were based on spherical

(36) Boudreaux, E. A.; Mulay, L. N. *Theory and Applications of Molecular Paramagnetism*; John Wiley and Sons: New York, 1976.
(37) Evans, D. F. *J. Chem. Soc.* **1958**, 2003.
(38) Damrauer, N. H.; Boussie, T. R.; Devenney, M.; McCusker, J. K. *J. Am. Chem. Soc.* **1997**, *119*, 8253.
(39) Crowley, C. E.; Clark, C. D.; Hoffman, M. Z. *Inorg. Chem.* **1998**, *37*, 5704.
(40) Clark, C. D.; Hoffman, M. Z. *Coord. Chem. Rev.* **1997**, *159*, 359.
(41) In Clark and Hoffman (cf. refs 39 and 40), k_q' corresponds to k_{et}, the electron transfer rate for the associated donor−acceptor complex. Our reasons for keeping the designation of this rate constant more general are discussed under Results and Discussion.

Table 1. Crystallographic Data for $Fe_2O(O_2CCF_3)_2(Tp)_2$ (**5**), $Fe_2O(O_2CCH_2OCH_3)_2(Tp)_2$ (**6**), $[Fe_2O(O_2CCH_2N(CH_3)_3)_2(Tp)_2](ClO_4)_2$ (**7**), and $[Fe_2OH(O_2CCH_2Cl)_2(Tp)_2](ClO_4)$ (**10**)

	5	**6**	**7**	**10**
empirical formula	$Fe_2O_5N_{13}C_{24}B_2H_{23}F_6$	$Fe_2O_7N_{12}C_{24}B_2H_{30}$	$Fe_2O_{13.5}C_{33.5}B_2H_{51.25}N_{16.75}Cl_2$	$Fe_2Cl_3C_{25}H_{31}N_{12}O_{10}B_2$
formula weight	820.83	731.89	1108.88	899.27
crystal color, habit	green, columnar	brown, blocks	red/green	red-orange, blocks
crystal system	orthorhombic	monoclinic	monoclinic	monoclinic
space group	Pnnm	$P2_1/c$	$C2$	$P2_1/n$
temperature (K)	156 ± 1	148 ± 1	123 ± 1	118 ± 1
cell dimensions:				
a (Å)	12.7895(6)	11.0086(3)	19.004(4)	11.6376(1)
b (Å)	15.1068(7)	14.2754(4)	23.757(5)	20.1514(5)
c (Å)	17.1456(8)	20.2699(6)	23.542(5)	15.4726(4)
β (deg)		101.751(1)	106.10(3)	91.487(1)
V (Å^3)	3312.7(2)	3118.70(14)	10212(4)	3627.32(11)
Z	4	4	8	4
D_{calc} (g cm^{-3})	1.646	1.559	1.443	1.647
goodness of fit (S)	1.41	0.90	0.977	0.90
R^a	0.033	0.030	0.0543	0.037
$R_w{}^b$	0.058	0.028	0.1126[c]	0.032

[a] $R = \sum||F_o| - |F_c||/\sum|F_o|$. [b] $R_w = (\sum\omega(|F_o| - |F_c|)^2/\sum F_o^2)^{1/2}$. [c] $wR_2 = \{\sum[\omega(F_o^2 - F_c^2)^2]/\sum[\omega(F_o^2)^2]\}^{1/2}$.

and elliptical models for the molecular volumes of the compounds, respectively, and were calculated using SPARTAN.[42]

X-ray Structure Determinations. Single-crystal X-ray structure determinations of $Fe_2O(O_2CCF_3)_2(Tp)_2$ (**5**), $Fe_2O(O_2CCH_2OCH_3)_2(Tp)_2$ (**6**), $[Fe_2O(O_2CCH_2N(CH_3)_3)_2(Tp)_2](ClO_4)_2$ (**7**), and $[Fe_2(OH)(O_2CCH_2Cl)_2(Tp)_2](ClO_4)$ (**10**) were carried out in the CHEXRAY facility of the University of California, Berkeley; crystallographic data are summarized in Table 1. Recrystallization from hot acetonitrile gave dark green X-ray quality crystals for **5**, **6**, and **7** while ether diffusion into dichloromethane gave orange-red crystals of **10**. Crystals were coated with Paratone N hydrocarbon oil, attached to glass fibers, transferred to a Siemens SMART diffractometer, and cooled in a dinitrogen stream. Lattice parameters were obtained from least-squares analyses. Crystals showed no significant decay during the data collection. Data were integrated and corrected for Lorentz and polarization effects, and analyzed for agreement and possible absorption using XPREP.[43] Space group assignments were based on systematic absences, packing considerations, a statistical analysis of intensity distribution, and successful refinement of the structures. The structures were solved by direct methods and were expanded using Fourier techniques. For the structures of **5**, **6**, and **10**, calculations were performed with the teXsan crystallographic software package of the Molecular Structure Corporation.[44] Due to the inability of teXsan to refine the Flack parameter, the final least-squares refinements for **7** were done with the SHELXTL software package.[43] Refinement of the twinning parameter in this case led to a final value of 0.50(1), indicating a perfect inversion twin. For structure **5**, all non-hydrogen atoms were refined anisotropically except for the fluorine atoms; the CF_3 groups were disordered and modeled appropriately. For structure **6**, all non-hydrogen atoms were refined anisotropically. For structure **7**, all non-hydrogen atoms were refined anisotropically while carbons were refined isotropically. For structure **10**, all non-hydrogen atoms were refined anisotropically except for the boron atoms, which were refined isotropically. For structures **5**, **6**, and **7**, the hydrogen atoms were included in calculated positions but not refined. Hydrogen atoms for **10** were located in the difference electron density map; the positions of these hydrogens, except for the hydroxide proton H1, were adjusted to give idealized bond distances and angles and were held fixed in the least-squares refinement. The position of H1 was refined, but its isotropic thermal parameter was held fixed. Further details of the structure determinations are deposited as Supporting Information.

Results and Discussion

Our research is focused on experimentally probing the correlation between spin exchange and chemical reactivity. The parent complex, $Fe_2O(O_2CCH_3)_2(Tp)_2$, was attractive because both the oxo- and hydroxo-bridged forms could be readily prepared and isolated. Protonation of the oxo bridge to form $[Fe_2(OH)(O_2CCH_3)_2(Tp)_2]^+$ results in a significant reduction in the magnitude of Heisenberg exchange between the two high-spin Fe^{III} sites. This system therefore provides two complexes that are quite similar in terms of their overall chemical composition yet differ substantially in the magnitude of intramolecular spin exchange.

The observed rate of decay from the photoexcited $[Ru(dmb)_3]^{2+}$ (^{3}MLCT state), k_{obs}, is given by

$$k_{obs} = k_0 + k_{en\ tr}[Q] + k_{et}[Q] \quad (2)$$

where [Q] is the concentration of quencher, k_0 is the rate of ^{3}MLCT decay in the absence of quencher, and $k_{en\ tr}$ and k_{et} are the rates of energy and electron transfer, respectively. In terms of differentiating energy and electron transfer, an examination of eq 3

$$[Ru(dmb)_3]^{2+} \xrightarrow{h\nu} [Ru(dmb)_3]^{2+}* \quad (3a)$$

$$[Ru(dmb)_3]^{2+}* + [Fe^{III}Fe^{III}] \xrightarrow[k_{en\ tr}]{} [Ru(dmb)_3]^{2+} + [Fe^{III}Fe^{III}]* \quad (3b)$$

$$[Ru(dmb)_3]^{2+}* + [Fe^{III}Fe^{III}] \xrightarrow[k_{et}]{} [Ru(dmb)_3]^{3+} + [Fe^{II}Fe^{III}] \quad (3c)$$

shows that deactivation of the ^{3}MLCT state produces different products depending on the nature of the quenching reaction: energy transfer yields an electronically excited Fe^{III} dimer ($[Fe^{III}Fe^{III}]$*, eq 3b), whereas electron transfer results in the formation of $[Ru(dmb)_3]^{3+}$ and a mixed-valent $Fe^{II}Fe^{III}$ species as redox photoproducts (eq 3c). The transient absorbance of a solution containing $[Ru(dmb)_3]^{2+}$ and $[Fe_2(OH)(O_2CCH_3)_2(Tp)_2]^+$ (**8**) at 440 nm following excitation at 450 nm is illustrated in Figure 1. It can be seen that the kinetics observed in the presence of **8** are biphasic in nature, in contrast to the monoexponential kinetics characteristic of simple ground-state recovery for $[Ru(dmb)_3]^{2+}$. Direct excitation of a solution of $[Fe_2(OH)(O_2CCH_3)_2(Tp)_2]^+$ in the absence of the Ru^{II} sensitizer revealed only pulse-width-limited transient features. Given our time

(42) *SPARTAN*, 4.0 ed.; Wavefunction, Inc.: Irvine, 1995.
(43) *XPREP*, 5.03 ed.; Siemens Industrial Automation, Inc.: Madison, 1995.
(44) *teXsan*; Molecular Structure Corporation, 1985 and 1992.

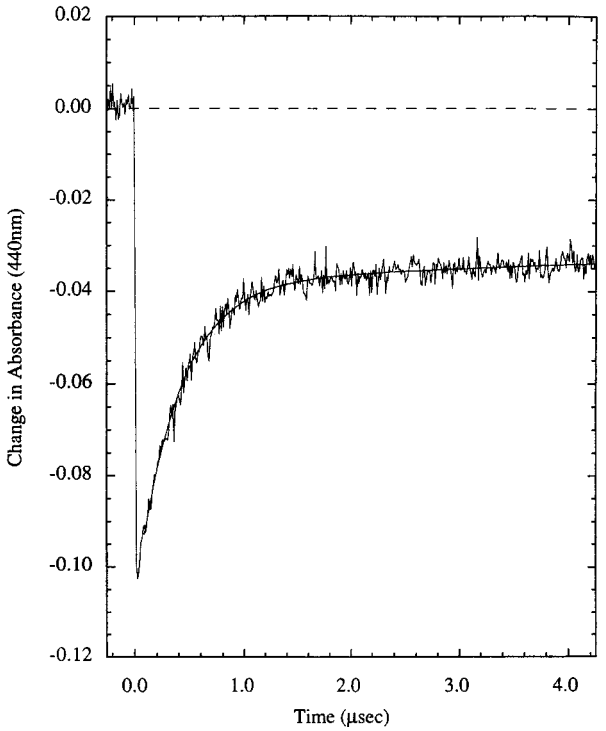

Figure 1. Plot of the excited-state differential absorbance of a CH_3CN solution containing $[Ru(dmb)_3]^{2+}$ ($\sim 5 \times 10^{-5}$ M) and $[Fe_2(OH)(O_2CCH_3)_2(Tp)_2]^+$ (2.7×10^{-4} M) at 440 nm following ~10 ns excitation at 450 nm. The solid line indicates a fit to a biexponential kinetic model. Although not shown in this figure, the trace returns completely to baseline in ~150 μs.

resolution, this indicates an electronic excited-state lifetime(s) of <10 ns for $[Fe_2(OH)(O_2CCH_3)_2(Tp)_2]^+$ in CH_3CN solution at 298 K.[45] The long-lived component in Figure 1 therefore cannot be ascribed to a $[Fe^{III}Fe^{III}]$* species. Accordingly, we attribute this slower component to the presence of electron transfer photoproducts, specifically, the kinetics of bimolecular charge recombination leading to reformation of the ground state (eq 4).

$$[Ru(dmb)_3]^{3+} + [Fe^{II}Fe^{III}] \xrightarrow{k_{bet}} [Ru(dmb)_3]^{2+} + [Fe^{III}Fe^{III}] \quad (4)$$

Analogous absorption measurements on solutions containing $[Ru(dmb)_3]^{2+}$ and $Fe_2O(O_2CCH_3)_2(Tp)_2$ revealed only the short-lived ^{3}MLCT transient observed in the emission quenching experiment; i.e., no long-lived feature attributable to bimolecular charge recombination was detected. This is likely due to a low cage-escape yield for this system and will be discussed in more detail later in the text.

Unfortunately, due to an inability to quantify the cage-escape yield for these reactions, measurements of the quantum yield for electron transfer could only afford a lower limit of ca. 25% in the case of quenching by $[Fe_2(OH)(O_2CCH_3)_2(Tp)_2]^+$; similar difficulties arise with the reactions to be discussed below. As a result, we cannot convert values of k_q' (eq 1) into unimolecular electron transfer rates.[41] However, the relative importance of these two reaction pathways can still be appreciated once the electron transfer chemistry has been described in full. Consequently, we now turn our attention to this aspect of the problem, after which the issue of energy transfer will be addressed.

(45) A similar result is found following photoexcitation of solutions containing only $Fe_2O(O_2CCH_3)_2(Tp)_2$.

Table 2. Reduction Potentials of $[Fe_2O(H)(O_2CR)_2(Tp)_2]^{n+}$ and Thermodynamic Driving Forces for Quenching of Various Ru^{II} Polypyridyl Sensitizers

		driving force for electron transfer[b] (eV)		
	E_{red} (V)[a]	$[Ru(bpy)_3]^{2+}$	$[Ru(dmb)_3]^{2+}$	$[Ru(tmb)_3]^{2+}$
Oxo-Bridged Dimers				
CH_3	−1.18	−0.04	−0.19	−0.30
CH_2OCH_3	−1.10	−0.12	−0.27	−0.38
CH_2F	−0.98	−0.23	−0.38	−0.49
CH_2Cl	−0.98	−0.24	−0.39	−0.50
$CHCl_2$	−0.83	−0.39	−0.54	−0.65
$CH_2N(CH_3)_3$	−0.76	−0.45	−0.61	−0.72
CF_3	−0.64	−0.57	−0.72	−0.84
Hydroxo-Bridged Dimers				
CH_3	−1.05	−0.16	−0.31	−0.43
CH_2F	−0.86	−0.36	−0.51	−0.63
CH_2Cl	−0.85	−0.37	−0.52	−0.63

[a] Reduction potentials are vs $Ag/AgNO_3$. Due to the irreversible nature of the electrochemistry, the values were taken as the peak current of the reduction scan. See text for further details. [b] Corrections to the driving force due to work terms (i.e., electrostatic) were calculated to be on the order of 10 meV, but were the same for all complexes in a given series. This correction has therefore not been incorporated into the values of ΔG_0 listed here since $\Delta\Delta G_0$ is not affected.

Scheme 1

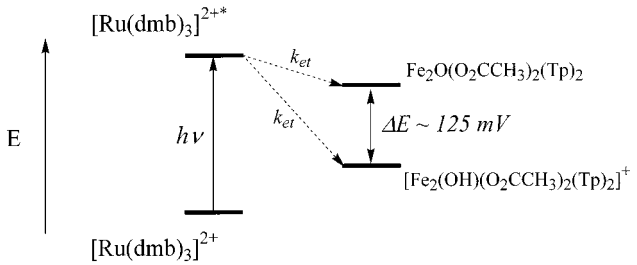

Deconvolving Electron Transfer Driving Force and Heisenberg Spin Exchange. The data presented in Figure 1 (as well as additional data to be described more fully in this section) unequivocally establish electron transfer as a viable mechanism in the quenching dynamics of these dinuclear Fe^{III} complexes. Decoupling the various factors that can influence electron transfer reactivity from spin exchange is therefore essential if the intrinsic effects of Heisenberg spin coupling are to be discerned. The semiclassical formulation of the Marcus equation for electron transfer is given in eq 5

$$k_{et} = \frac{4\pi^2}{h}|H_{ab}|^2(4\pi\lambda k_b T)^{-1/2} \exp\left(\frac{-(\Delta G_0^{ET} + \lambda)^2}{4\lambda k_b T}\right) \quad (5)$$

where ΔG_0^{ET} is the electron transfer driving force, λ is the total reorganization energy, and H_{ab} is the electronic coupling between the donor and acceptor. The effect protonation of the oxo bridge has on the driving force for electron transfer is evident from the electrochemical properties of the oxo- and hydroxo-bridged dimers; these data are presented in Table 2. The ca. 125 mV positive shift in the reduction potential of the dimer upon protonation implies an increase in the driving force for electron transfer in the case of $[Fe_2(OH)(O_2CCH_3)_2(Tp)_2]^+$ relative to $Fe_2O(O_2CCH_3)_2(Tp)_2$ (Scheme 1). The thermodynamic consequences of protonation are therefore an issue that must be addressed: the larger driving force for electron transfer

to the hydroxo-bridged dimer could, in principle, account for the increase in k_q' exclusive of changes in spin exchange.[46]

Variations in driving force can be realized by changing the redox properties of either the sensitizer or the quencher. In the case of the former, it is well documented that the reduction potential of the ^{3}MLCT excited state of Ru^{II} polypyridyl complexes can be modified through derivatization of the bipyridyl rings.[47] $[Ru(bpy)_3]^{2+}$ and $[Ru(tmb)_3]^{2+}$ (where tmb is 4,4′,5,5′-tetramethyl-2,2′-bipyridine) were therefore chosen to augment $[Ru(dmb)_3]^{2+}$ as sensitizers. These specific compounds were selected in order to minimize changes in donor contributions to the reorganization energy. Calculated driving forces to $Fe_2O(O_2CCH_3)_2(Tp)_2$ were found to be -0.036, -0.188, and -0.302 eV for sensitization by $[Ru(bpy)_3]^{2+}$, $[Ru(dmb)_3]^{2+}$, and $[Ru(tmb)_3]^{2+}$, respectively.[48] Although the quenching rate across this series does show the expected increase with increasing driving force (vide infra), the range of driving force is relatively small. If we consider that the reorganization energy for self-exchange of $[Ru(bpy)_3]^{2+}$ in CH_3CN is approximately 0.4 eV (and thus the reorganization energy of the overall reaction we are considering is at least this large),[49] then a $\Delta\Delta G_0$ spanning 0.266 eV samples only a limited region of the associated Marcus curve for the reaction.

A possible means for altering the redox potential of the dinuclear acceptors was suggested by the work of Wieghardt and co-workers.[50] In similar oxo-bridged dinuclear Ru^{III} complexes, it was demonstrated that substantial shifts in the reduction potential of the cluster could be obtained by changing the bridging carboxylates. Obviously this approach will only be helpful in the present circumstance if the magnitude of spin coupling between the Fe^{III} centers is insensitive to such a change. The large number of examples of oxo-biscarboxylato-bridged dimers that have been prepared by other workers reveal that the nature of the ancillary ligands (e.g., Tp, TACN, bis(2-pyridylmethyl)amine, etc.) and bridging carboxylate have little if any impact on the magnitude of Heisenberg exchange between the metal ions.[51−56] Gorun and Lippard have in fact used these data to demonstrate that it is largely the $Fe^{III}-O_{bridge}$ distance that dictates the strength of exchange coupling in such compounds.[57,58] Theoretical work by Brown and Solomon,[59] as well as our own density functional calculations,[60] further support the notion that superexchange in this class of molecules is dominated by interactions between the metal centers and the oxo/hydroxo bridge. Varying the carboxylate bridge in these ferric clusters may therefore provide the mechanism needed for tuning the driving force for photoinduced electron transfer independent of spin exchange.

Accordingly, we have prepared a series of oxo- and hydroxo-bridged dinuclear $Fe^{III}Fe^{III}$ complexes of the form $[Fe_2O(H)(O_2CR)_2(Tp)_2]^{0,+}$. As R groups, we chose CH_2OCH_3, CH_2F, CH_2Cl, $CHCl_2$, and CF_3 to complement the CH_3 system already studied; an additional complex containing the cationic $CH_2N^+(CH_3)_3$ moiety was also prepared in order to investigate charge effects (vide infra). Whereas oxo-bridged complexes of all of these carboxylates could be readily prepared and isolated, only complexes with R = CH_3, CH_2F, and CH_2Cl afforded hydroxo-bridged analogues that were stable in solution. Electrochemical data collected on all of the oxo- and hydroxo-bridged complexes making up our study are compiled in Table 2. As with the acetate-bridged compounds, all of the newly prepared complexes exhibited irreversible reduction waves by cyclic voltammetry. However, since we are interested in relative changes in driving force, we can take the potential at the peak reduction current as a measure of the cluster's potential for comparative purposes.[61] The total variation in reduction potential is >550 mV, with the CH_3 and CF_3 compounds lying at the two extremes of the series. Combined with the three Ru^{II} polypyridyl sensitizers mentioned above, a nearly 900 meV variation in the driving force for photoinduced electron transfer is realized. The important point to note is that quenching measurements can now be carried out for which the driving force for electron transfer to an oxo-bridged acceptor exceeds that of a hydroxo-bridged acceptor.

Magnetic susceptibility measurements were carried out on all compounds in order to experimentally assess the impact of carboxylate variation on spin exchange within the dimers. These data are collected in Table 3; plots of effective moment versus temperature for $Fe_2O(O_2CCH_2Cl)_2(Tp)_2$ and $[Fe_2(OH)(O_2CCH_2Cl)_2(Tp)_2]^+$ are shown in Figure 2 as examples. The magnitude of exchange coupling for $Fe_2O(O_2CCH_2Cl)_2(Tp)_2$ was determined to be -120 cm^{-1}.[62] This is identical, within experimental error, to that obtained for $Fe_2O(O_2CCH_3)_2(Tp)_2$. An inspection of Table 3 reveals that the spin exchange integrals for all of the oxo-bridged compounds lie in the range of $J = -119 \pm 4$ cm^{-1}. Values for μ_{eff} in solution are also constant across the series in room-temperature CH_3CN solution and, moreover, are the same in each case as those found in the solid state.[63] Analogous results were observed for the hydroxo-bridged compounds: although this series has fewer members, all of the measured spin exchange integrals are ca. -18 ± 2 cm^{-1} and in each case exhibit identical

(46) The redox shift could be related to the change in Heisenberg spin coupling upon protonation, as suggested by Bertrand and Gayda (cf. ref 11). However, we cannot assume a priori that this is the case.
(47) Juris, A.; Baragelletti, S.; Campagna, S.; Balzani, V.; Belser, P.; von Zelewski, A. *Coord. Chem. Rev.* **1988**, *84*, 85.
(48) The driving force for electron transfer from the ^{3}MLCT state of the Ru^{II} chromophore to the quencher can be calculated from the redox properties of the donor and acceptor and the zero-point energy (E_0) of the ^{3}MLCT state. Values of E_0 were obtained from the analyses of the emission spectra of the three sensitizers as described elsewhere (cf. ref 38).
(49) Young, R. C.; Keene, F. R.; Meyer, T. J. *J. Am. Chem. Soc.* **1977**, *99*, 2468.
(50) Neubold, P.; Wieghardt, K.; Nuber, B.; Weiss, J. *Inorg. Chem.* **1989**, *28*, 459.
(51) Lee, D. W.; Lippard, S. J. *J. Am. Chem. Soc.* **1998**, *120*, 12153−12154.
(52) Menage, S.; Brennan, B. A.; Juarezgarcia, C.; Munck, E.; Que, L. *J. Am. Chem. Soc.* **1990**, *112*, 6423−6425.
(53) Mizoguchi, T. J.; Lippard, S. J. *J. Am. Chem. Soc.* **1998**, *120*, 11022−11023.
(54) Que, L.; Dong, Y. H. *Acc. Chem. Res.* **1996**, *29*, 190−196.
(55) Watton, S. P.; Masschelein, A.; Rebek, J.; Lippard, S. J. *J. Am. Chem. Soc.* **1994**, *116*, 5196−5205.
(56) Beer, R. H.; Tolman, W. B.; Bott, S. G.; Lippard, S. J. *Inorg. Chem.* **1991**, *30*, 2082−2092.
(57) Gorun, S. M.; Lippard, S. J. *Inorg. Chem.* **1991**, *30*, 1625−1630.
(58) The influence of bond angle has also been addressed. See: Weihe, H.; Gudel, H. U. *J. Am. Chem. Soc.* **1997**, *119*, 6539−6543.
(59) Brown, C. A.; Remar, G. J.; Musselman, R. L.; Solomon, E. I. *Inorg. Chem.* **1995**, *34*, 688.
(60) Rodriguez, J. H.; McCusker, J. K. Submitted for publication.
(61) Values for the peak reduction potentials were found to depend on scan rate, exhibiting a −40 mV shift upon increasing the scan rate from 100 to 500 mV/s. However, all complexes in a given series showed the exact same scan rate dependence; i.e., differences in reduction potential were independent of scan rate. The differences in reduction potential between any oxo/hydroxo pair was likewise independent of scan rate. The same reduction potential differences derived from the cyclic voltammetry data in Table 2 were also obtained from square wave voltammetry measurements for several of the oxo- and hydroxo-bridged complexes.
(62) The data were fit to an effective spin Hamiltonian of the form $\mathbf{H} = -2J\mathbf{S}_T^2$, where J is the scalar spin exchange integral and $\mathbf{S}_T = \mathbf{S}_1 + \mathbf{S}_2$. All fits were carried out with a fixed value of $g = 2.00$ and TIP on the order of 1×10^{-4}.
(63) Addition of H_2O to these solutions did not affect the measured values of μ_{eff}.

Table 3. Magnetic Susceptibility Data for $[Fe_2O(H)(O_2CR)_2(Tp)_2]^{n+}$ Complexes

		μ_{eff}	
	J (cm^{-1})[a]	solid[b]	solution[b,c]
	Oxo-Bridged Dimers		
CH_3	−117	2.40	2.41 ± 0.2
CH_2OCH_3	−118	2.54	2.68 ± 0.2
CH_2F	−119	2.45	2.58 ± 0.2
CH_2Cl	−120	2.43	2.43 ± 0.2
$CHCl_2$	−118	2.50	2.52 ± 0.2
$CH_2N(CH_3)_3$	−124	2.46	*d*
CF_3	−115	2.56	2.53 ± 0.2
	Hydroxo-Bridged Dimers		
CH_3	−17	6.06	5.93 ± 0.2
CH_2F	−19	6.03	5.90 ± 0.2
CH_2Cl	−19	6.04	5.89 ± 0.2

[a] All fits were carried out assuming a spin Hamiltonian of the form $\mathbf{H} = -2J\mathbf{S}_1\cdot\mathbf{S}_2$ with g fixed at 2.00 and TIP values on the order of 1×10^{-4}. [b] Values correspond to 300 K. [c] Measurements made in $CDCl_3$ solutions. [d] Compound was not sufficiently soluble in $CDCl_3$.

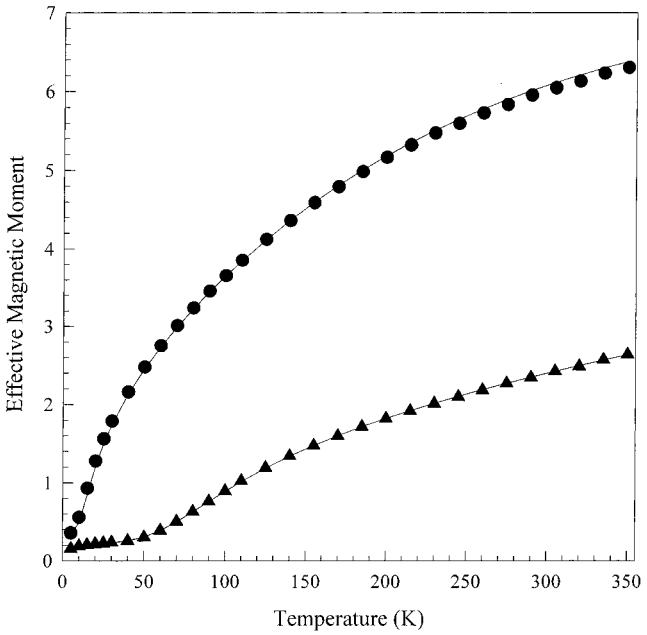

Figure 2. Plots of effective magnetic moment versus temperature for $Fe_2O(O_2CCH_2Cl)_2(Tp)_2$ (triangles) and $[Fe_2(OH)(O_2CCH_2Cl)_2(Tp)_2](ClO_4)$ (circles) in the solid state. The solid lines represent theoretical fits of the data. See text for further details.

values of μ_{eff} at room temperature in both solution and the solid state.[63] We therefore conclude that changing the carboxylate bridge does not significantly perturb exchange interactions present in the ground states of these molecules.

With this more extensive set of compounds, we have the means to examine the reactivity of exchange-coupled transition metal complexes over a wide range of electron transfer driving force independent of changes in the spin exchange properties of the system. Quenching rates were again determined from nanosecond time-resolved emission measurements. The observation of biphasic ground-state recovery kinetics in the case of quenching by $Fe_2O(O_2CCF_3)_2(Tp)_2$ using $[Ru(tmb)_3]^{2+}$ as the sensitizer as well as $[Fe_2(O_2CCH_2N(CH_3)_3)_2(Tp)_2]^{2+}$ with all three sensitizers are points worth noting. The reaction sequences of interest are depicted in Scheme 2. For diffusional charge recombination to be observed, dissociation of the associated donor/acceptor complex after electron transfer (k_{D2}) must be kinetically competitive with k_{BET}'. We suggested above that the absence of bimolecular charge recombination for quenching of

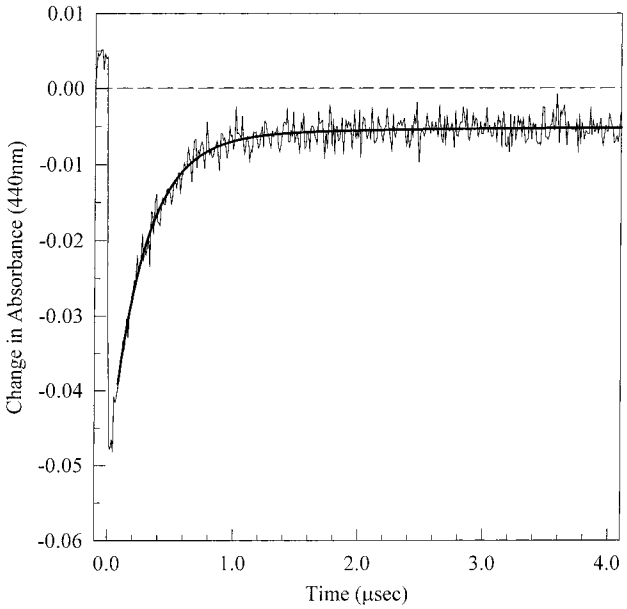

Figure 3. Plot of the excited-state differential absorbance of a CH_3CN solution containing $[Ru(tmb)_3]^{2+}$ ($\sim 5 \times 10^{-5}$ M) and $Fe_2O(O_2CCF_3)_2(Tp)_2$ (7.6×10^{-4} M) at 440 nm following ~10 ns excitation at 450 nm. The data show a long-lived component ascribed to charge recombination following photoinduced electron transfer.

Scheme 2

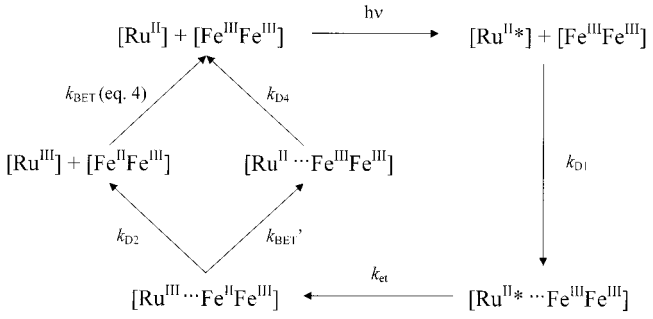

$[Ru(dmb)_3]^{2+}$ by $Fe_2O(O_2CCH_3)_2(Tp)_2$ was due to rapid back-electron transfer, a reaction that would be facilitated by the ion pair that is formed following electron transfer to the oxo-bridged dimers. The observation of the charge-separated species for quenching by $[Fe_2(O_2CCH_2N(CH_3)_3)_2(Tp)_2]^{2+}$ is consistent with this model: in this case, electron transfer results in the formation of a cationic (as opposed to anionic) acceptor, thereby favoring dissociation of the product donor/acceptor pair via k_{D2}. Additional support for electron transfer occurring in all of the oxo-bridged systems comes from data acquired for quenching of $[Ru(tmb)_3]^{2+}*$ by $Fe_2O(O_2CCF_3)_2(Tp)_2$. A plot of the single-wavelength excited-state absorption difference spectrum for this system is illustrated in Figure 3. This system has the largest driving force of all the reactions studied (−0.836 eV), and will therefore have the smallest free energy change for back-electron transfer. This will increase k_{D2}/k_{BET}' via reduction of k_{BET}', thereby favoring formation of the separated ion pair.

Quenching data obtained for all of the compounds in this study are given in Table 4 with a plot of ΔG_0^{ET} versus $\ln k_q'$ illustrated in Figure 4. We consider first the data for the oxo-bridged quenchers. It can be seen that the rate shows a significant dependence on the electron transfer driving force of the reaction. Since we are still formally dealing with k_q' (eq 1), it is not possible to fit these data to eq 5. However, it is clear that the qualitative behavior of the oxo-bridged complexes is consistent with Marcus normal region type behavior. Of

Table 4. Bimolecular (k_q) and Diffusion-Corrected (k_q') Quenching Rates for $[Fe_2O(H)(O_2CR)_2(Tp)_2]^{n+}$ Using Various Ru^{II} Polypyridyl Sensitizers[a]

	$[Ru(bpy)_3]^{2+}$		$[Ru(dmb)_3]^{2+}$		$[Ru(tmb)_3]^{2+}$	
	k_q ($\times 10^9$ M^{-1} s^{-1})	k_q' ($\times 10^9$ s^{-1})	k_q ($\times 10^9$ M^{-1} s^{-1})	k_q' ($\times 10^9$ s^{-1})	k_q ($\times 10^9$ M^{-1} s^{-1})	k_q' ($\times 10^9$ s^{-1})
Oxo-Bridged Dimers						
CH_3	0.80	0.22	0.78	0.20	1.80	0.48
CH_2OCH_3	1.11	0.30	1.10	0.27	2.34	0.61
CH_2F	1.60	0.46	1.80	0.47	3.10	0.87
CH_2Cl	1.60	0.45	1.90	0.49	3.50	0.99
$CHCl_2$	2.90	0.86	3.30	0.91	4.60	1.37
$CH_2N(CH_3)_3$	1.46	1.92	1.74	1.94	2.45	2.91
CF_3	4.10	1.32	4.20	1.24	6.00	1.98
Hydroxo-Bridged Dimers						
CH_3	4.80	4.10	5.00	3.72	5.50	4.27
CH_2F	5.20	4.54	6.20	5.06	5.80	4.56
CH_2Cl	5.60	4.93	5.90	4.58	6.20	4.94

[a] Error bars for the rate constants are estimated to be ±10% based on repeated measurements.

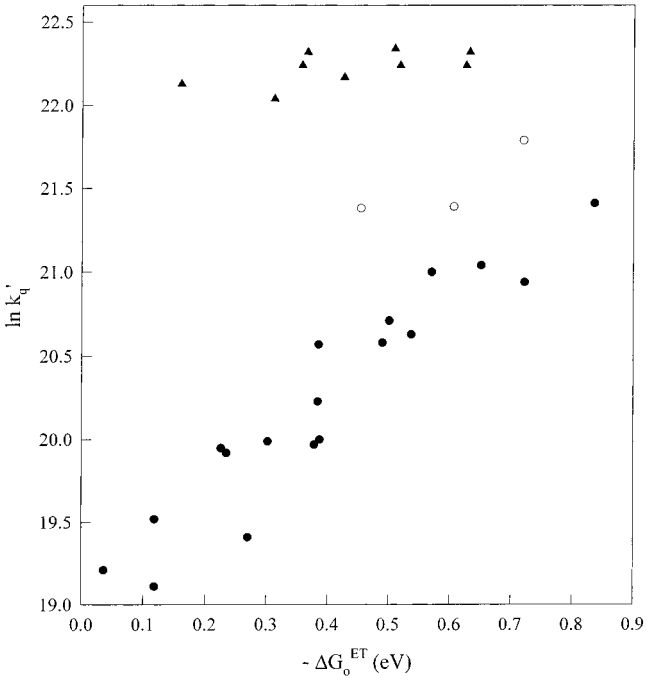

Figure 4. Plot of the diffusion-corrected quenching rates (as ln k_q') versus electron transfer driving force (ΔG_0^{ET}) for the reaction of photoexcited Ru^{II} polypyridyl complexes with $Fe_2O(O_2CR)_2(Tp)_2$ (circles) and $[Fe_2(OH)(O_2CR)_2(Tp)_2]^+$ (triangles). The open circles correspond to data for R = $CH_2N(CH_3)_3$.

particular note are the quenching rates for $[Fe_2O(O_2CCH_2N(CH_3)_3)_2(Tp)_2]^{2+}$. Although slightly larger than other oxo-bridged systems of comparable driving force, k_q' values for this compound still fall below that of any hydroxo-bridged species. This suggests that overall molecular charge plays only a minor role in the reaction dynamics of these systems.

A similar correlation between ΔG_0^{ET} and ln k_q' is not evident in the case of the hydroxo-bridged quenchers. The relative insensitivity of the observed rate to the driving force for electron transfer in these systems is indicative of a diffusion-limited reaction and/or the dominance of an energy transfer process whose rate is independent of the redox potentials of the molecules. Diffusion-limited reactions in CH_3CN occur on the order of 10^9-10^{10} M^{-1} s^{-1}.[64] Our quenching rates are therefore consistent with these values, albeit lying at the lower end of this range. This observation, in conjunction with our assessment of the role energy transfer plays in the reactivity of the hydroxo-bridged dimers in particular (vide infra), compels us to ascribe this lack of driving force dependence to diffusion. Values of k_q' for the hydroxo-bridged quenchers must therefore be viewed as lower limits on their reaction rates.

The utility of having driving force variability for the oxo- and hydroxo-bridged dimers is the prospect of being able to compare the reactivity of any member of one series with any member of the other. In order for this approach to be valid, the reorganization energy associated with each member of a given series must be the same. Since we do not have values for k_{et}, variable-temperature quenching studies do not provide an experimental means for determining λ directly. However, contributions to λ for reactions involving the oxo- versus hydroxo-bridged dimers can be reasonably inferred from crystallographic data (inner sphere, λ_{in}) and considerations from dielectric continuum theory (outer sphere, λ_{out}).

We have carried out single-crystal X-ray structure determinations of $Fe_2O(O_2CCF_3)_2(Tp)_2$ (**5**), $Fe_2O(O_2CCH_2OCH_3)_2(Tp)_2$ (**6**), $[Fe_2O(O_2CCH_2N(CH_3)_3)_2(Tp)_2]^{2+}$ (**7**), and $[Fe_2(OH)(O_2CCH_2Cl)_2(Tp)_2]^+$ (**10**) to augment the previously published crystal structures of $Fe_2O(O_2CCH_3)_2(Tp)_2$ (**1**)[31] and $[Fe_2(OH)(O_2CCH_3)_2(Tp)_2]^+$ (**8**).[32] Selected bond lengths and angles for all of these complexes are listed in Table 5. Figure 5 shows an ORTEP diagram of **5** along with the labeling scheme used in Table 5. The data in Table 3 indicate that the strength of exchange coupling is essentially independent of the identity of the bridging carboxylate. Since the spin exchange interaction is expected to be sensitive to the Fe−O_{bridge} distance, we anticipate that the Fe−O_{bridge} bond length will be constant across this series. An examination of Table 5 shows that this is in fact the case: bond length variations span a relatively narrow range of 0.016 Å. Although the limits of this range are defined by the two extremes with respect to reduction potential (i.e., compounds **1** (1.780(2) Å) and **5** (1.796(1) Å)), the data in Table 5 do not reveal any clearly identifiable trend between the Fe−O_{bridge} bond length and electron withdrawing/donating capability of the parent carboxylic acid. The remaining bond distances and angles show only small variations across the series for a given bond type. In particular, we note that the Fe−O_{bridge}−Fe angle spans less than 1°, from 125.75(14)° in **1** to 126.6(3)° in **6**. An analogous comparison can be made between the two hydroxo-bridged complexes. We note that the Fe−$(OH)_{bridge}$ bond length is slightly shorter for the compound containing the more electron withdrawing carboxylate (1.940(4) Å for **10** vs 1.960(4) Å for **8**). Unfortunately, with only two examples it is difficult to determine if this is representative of a trend or simply a statistical variation. The Fe−N bond distances are all very

(64) Rehm, D.; Weller, A. *Isr. J. Chem.* **1970**, *8*, 259.

Table 5. Selected Bond Distances (Å) and Angles (deg) for $Fe_2O(O_2CR)_2(Tp)_2$ (R = CH_3 (**1**), CF_3 (**5**), CH_2OCH_3 (**6**), $CH_2N(CH_3)_3$ (**7**) and $[Fe_2OH(O_2CR)_2(Tp)_2](ClO_4)$ (R = CH_3 (**8**), CH_2Cl (**10**))

	oxo bridged				hydroxo bridged	
	1[a]	**5**	**6**	**7**	**8**[b]	**10**
			Bond Distances (Å)			
Fe1−O1	1.783(2)	1.796(1)	1.790(2)	1.787(5)	1.960(4)	1.940(4)
Fe2−O1	1.788(2)	*c*	1.790(2)	1.772(5)	1.952(4)	1.942(4)
Fe1−N(a)[d]	2.153(3)	2.114(3)	2.142(3)	2.118(6)	2.108(5)	2.095(4)
Fe1−N(b)[d]	2.154(3)	2.114(3)	2.161(3)	2.095(6)	2.088(4)	2.079(4)
Fe1−N(c)[d]	2.197(3)	2.155(3)	2.212(3)	2.169(6)	2.110(5)	2.111(4)
Fe2−N(d)[d]	2.150(3)	*c*	2.162(3)	2.114(6)	2.094(4)	2.091(4)
Fe2−N(e)[d]	2.149(3)	*c*	2.128(3)	2.132(6)	2.108(4)	2.088(4)
Fe2−N(f)[d]	2.177(3)	*c*	2.164(3)	2.195(6)	2.105(4)	2.115(4)
			Bond Angles (deg)			
Fe1−O1−Fe2	123.54(4)	130.9(2)	125.75(14)	126.6(3)	123.007(2)	123.89(18)
O1−Fe1−O2	96.571(4)	93.0(1)	95.61(10)	94.6(2)	92.772(2)	91.95(16)
O2−Fe1−O3	91.853(4)	93.80(9)	94.84(10)	88.2(1)	91.112(2)	88.68(15)
O1−Fe1−O3	97.101(4)	92.7(1)	95.25(2)	95.8(2)	91.139(2)	90.76(15)

[a] Data taken from ref 31. [b] Data taken from ref 32. [c] Values have been omitted because the molecule lies on a mirror plane and thus only half the dimer is crystallographically unique. [d] Numbering schemes for each molecule are slightly different. Identical bonds are being compared in this table; specific numbering schemes for each compound can be found in the Supporting Information.

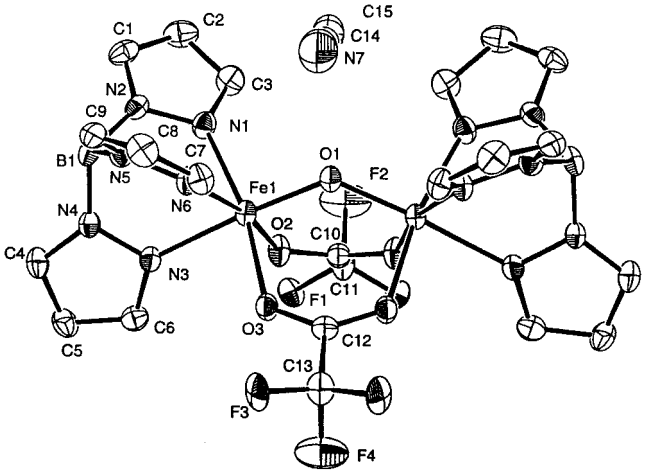

Figure 5. Drawing of $Fe_2O(O_2CCF_3)_2(Tp)_2$ (**5**) obtained from a single-crystal X-ray structure determination. See Table 1 for crystallographic details and Table 5 for metric details.

similar and unremarkable for both compounds, as are the bond angles. Based on these structural comparisons, we conclude that metric variations within each series (i.e., oxo- or hydroxo-bridged) are minimal in response to changing the identity of the bridging carboxylate. We therefore do not expect significant differences among various members of a given series in their contribution to the structural reorganization energies.

The relevant issue with regard to electron transfer dynamics is the change in structure and/or solvation of the dinuclear Fe^{III} compounds upon reduction and whether that change is modulated due to protonation of the oxo bridge. A specific comparison of all of the structures relevant for the reaction in question is not possible because reductions of both $Fe_2O(O_2CR)_2(Tp)_2$ and $[Fe_2(OH)(O_2CR)_2(Tp)_2]^+$ result in decomposition into monomeric $[Fe(Tp)_2]^{0/+}$ complexes. However, the necessary oxidation levels are attainable in an analogous system that replaces Tp with 1,4,7-trimethyl-1,4,7-triazacyclononane (Me_3TACN) as a capping ligand.[65,66] Table 6 lists the $Fe-O_{bridge}$ bond lengths for molecules in the oxidation states of interest. It can be seen that the $Fe-O_{bridge}$ distance for the oxo-bridged $[Fe^{III}Fe^{III}]$ form is the same for both the Tp and Me_3TACN complexes. Upon reduction, two $Fe-O_{bridge}$ distances are reported for the Me_3-TACN complex reflecting the largely valence-localized nature of the compound. The longer of the two bonds at 1.844(4) Å was assigned as the $Fe^{II}-O_{bridge}$ distance, with the $Fe^{III}-O_{bridge}$ somewhat shorter at 1.818(4) Å. From these values we can estimate a ca. 0.04−0.05 Å increase in the $Fe-O_{bridge}$ bond distance upon reduction of $Fe_2O(O_2CR)_2(Tp)_2$ complexes in forming the mixed-valent photoproduct. Metric details for a structurally characterized hydroxo-bridged $[Fe^{II}Fe^{III}]$ complex reveal an $Fe^{II}-(OH)$ distance of 2.005 Å.[67] The total bond distance change upon reduction of the $Fe^{III}-(OH)$ moiety is therefore also 0.04−0.05 Å. Although we have chosen here to focus primarily on the $Fe-O_{bridge}$, the comparison nevertheless suggests that differences in the inner-sphere reorganization energy should be minimal for electron transfer to oxo- versus hydroxo-bridged quenchers since the changes in internal coordinates for reduction of both complexes are similar.[68] The outer-sphere contribution (λ_{out}) can be estimated from a dielectric continuum model. However, since all of the reactions studied involve the same net transfer of charge, were carried out in the same solvent, and involve structurally homologous donors and acceptors, differences in λ_{out} should be negligible.[69]

On the basis of the above considerations, there is little reason to expect significantly different values of λ for electron transfer quenching by oxo- versus hydroxo-bridged Fe^{III} dimers. Given this, the series we have described constitutes a mechanism for decoupling both electron transfer driving force and reorganization energy from spin exchange in quenching reactions involving these two classes of complexes. The utility of this lies in the comparisons we can now make between oxo- (large exchange) and hydroxo- (small exchange) bridged quenchers. The dependence on driving force illustrated in Figure 4 clearly demonstrates that the difference in reactivity between the oxo- and hydroxo-bridged systems is *not* a trivial manifestation of the change in reduction potential of the cluster upon protonation: there are numerous comparisons that can be made for which an

(65) Lachicotte, R.; Kitaygorodskiy, A.; Hagen, K. S. *J. Am. Chem. Soc.* **1993**, *115*, 8883−8884.
(66) Cohen, J. D.; Payne, S.; Hagen, K. S.; Sanders-Loehr, J. *J. Am. Chem. Soc.* **1997**, *119*, 2960−2961.
(67) Bossek, U.; Hummel, H.; Weyhermuller, E. B.; Wieghardt, K. *Angew. Chem., Int. Ed. Engl.* **1995**, *34*, 2642−2645.
(68) There will be a slight difference in λ_{in} for the oxo- and hydroxo-bridged dimers for a given Δr_{Fe-O} due to the smaller force constant expected for the hydroxo-bridged dimer.
(69) In the case of R = $CH_2N(CH_3)_3$, one should expect a slight difference in λ_{out} due to the additional charge associated with the oxo-bridged complex.

Table 6. Iron−Oxo/Hydroxo Bond Length Comparison for [$Fe^{III}Fe^{III}$] and [$Fe^{II}Fe^{III}$] Complexes[a]

	isovalent $Fe^{III}Fe^{III}$	mixed-valent $Fe^{II}Fe^{III}$	
	$Fe^{III}-O_{bridge}$	$Fe^{III}-O_{bridge}$	$Fe^{II}-O_{bridge}$
	Oxo-Bridged Dimers		
$Fe_2O(O_2CCH_3)_2(Tp)_2$[b]	1.780(2), 1.788(2)	–	–
$Fe_2O(O_2CCF_3)_2(Tp)_2$[c]	1.796(1), 1.796(1)	–	–
$[Fe_2O(O_2CC(Ph_3))_2(Me_3TACN)_2]^{2+/+}$[d]	1.796(3), 1.792(3)	1.818(4)	1.844(4)
	Hydroxo-Bridged Dimers		
$[Fe_2(OH)(O_2CCH_3)_2(Tp)_2]^+$[e]	1.960(4), 1.952(4)	–	–
$[Fe_2(OH)(O_2CCH_2Cl)_2(Tp)_2]^+$[c]	1.940(4), 1.942(4)	–	–
$[Fe_2(OH)(piv)_2(Me_3TACN)_2]^{+/0}$[f]	–	1.961(5)	2.005(5)

[a] Values reported in Å. [b] Taken from ref 31. [c] This work. [d] Taken from ref 66. [e] Taken from ref 32. [f] Taken from ref 67.

oxo-bridged complex has a larger driving force for electron transfer than a hydroxo-bridged complex, yet exhibits a slower quenching rate. For example, k_q' for quenching of $[Ru(tmb)_3]^{2+}$ by $Fe_2O(O_2CCH_2Cl)_2(Tp)_2$ is a factor of ca. 4 slower than the (diffusion-limited) rate found for the $[Ru(bpy)_3]^{2+}$/$[Fe_2(OH)(O_2CCH_3)_2(Tp)_2]^+$ pair despite having a 0.340 eV larger driving force. Electron transfer quenching of $[Ru(bpy)_3]^{2+}$* by $Fe_2O(O_2CCHCl_2)_2(Tp)_2$ will occur with approximately the same driving force and reorganization energy as $[Fe_2(OH)(O_2CCH_2Cl)_2(Tp)_2]^+$, but the quenching rates associated with these two complexes differ by nearly a factor of 6 at room temperature (8.60×10^8 s^{-1} versus 4.93×10^9 s^{-1}, with the latter representing the diffusion limit for the reaction). We therefore conclude that the driving force and reorganization energy for electron transfer, while certainly important in a general sense, are not the principal reasons behind differences in quenching rates between these two types of exchange-coupled systems.

Energy Transfer. We now turn our attention to the issue of energy transfer. As indicated previously, the difficulty in obtaining an accurate assessment of the cage-escape yield for these bimolecular reactions precludes us from quantifying the relative contributions of energy and electron transfer to the reactivity of the oxo- and hydroxo-bridged dimers. Nevertheless, spectral overlap considerations immediately rule out any contribution to the quenching of $[Ru(dmb)_3]^{2+}$* by $[Fe_2(OH)(O_2CR)_2(Tp)_2]^+$ from a through-space dipolar mechanism (Figure 6). Such is not the case for $Fe_2O(O_2CR)_2(Tp)_2$, however, where the oxo-to-metal LMCT band and emission spectrum of the sensitizer have an appreciable cross section: resonant energy transfer via dipolar coupling is therefore a distinct possibility for this class of compounds. To understand what this implies in terms of the relative reactivities of these molecules, we can rewrite the expression for the observed quenching rate constant, eq 2, to reflect the two possible contributing energy transfer mechanisms:

$$k_{obs} = k_0 + k_{et}[Q] + k_{en\ tr}[Q] \quad (6)$$

$$= k_0 + k_{et}[Q] + (k_F + k_D)[Q] \quad (6a)$$

In eq 6a, k_F and k_D are Förster and Dexter transfer rates, respectively. Again, based on the lack of any spectral overlap between the ruthenium emission and absorption of the hydroxo-bridged dimers, $k_F \approx 0$. Thus, the difference in quenching rates between oxo- and hydroxo-bridged reactants at constant quencher concentration can be expressed as in eq 7

$$k_{obs}^{(hydroxo)} - k_{obs}^{(oxo)} = \{(k_{et}^{(hydroxo)} - k_{et}^{(oxo)}) + (k_D^{(hydroxo)} - (k_F^{(oxo)} + k_D^{(oxo)}))\}[Q] \quad (7)$$

where $k_i^{(j)}$ refers to the relevant rate constant for the hydroxo- or oxo-bridged quencher, as indicated.

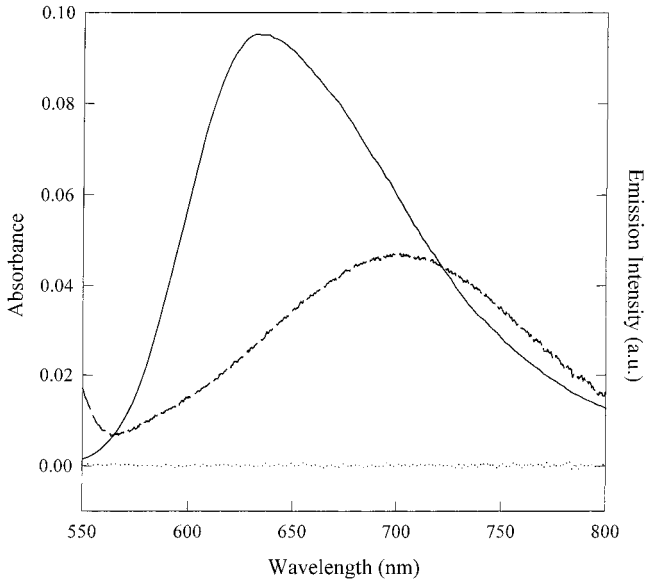

Figure 6. Overlay of the absorption spectra of $Fe_2O(O_2CCH_3)_2(Tp)_2$ (dashed line) and $[Fe_2(OH)(O_2CCH_3)_2(Tp)_2]^+$ (dotted line), measured in CH_3CN at equal concentrations, with the room-temperature emission spectrum of $[Ru(dmb)_3]^{2+}$ in CH_3CN (solid line).

Under conditions for which both the driving force and reorganization energy for electron transfer are constant, the data presented in Figure 4 clearly show that hydroxo-bridged dimers quench more efficiently than oxo-bridged dimers. Since the contribution from Förster transfer is negligible for the hydroxo-bridged complexes (Figure 6), it must therefore be the case that Dexter and/or electron transfer to the hydroxo-bridged complexes is significantly faster than to the oxo-bridged dimers i.e., $k_D^{(hydroxo)} > k_D^{(oxo)}$ and/or $k_{et}^{(hydroxo)} > k_{et}^{(oxo)}$. The relative importance of these two mechanisms for oxo/hydroxo reactivity difference can be further assessed with the data in Figure 4. It has been demonstrated that the initial slope of the Marcus curve, $\delta(RT \ln k)/\delta(\Delta G)$, should equal 0.5 if the rate constant k describes a pure electron transfer process.[70] The slope calculated from Figure 4 for quenching by the oxo-bridged complexes[71] is 0.08. From this result two inferences are immediately drawn. First, energy transfer does, in fact, contribute to excited-state quenching in the case of the oxo-bridged dimers. Given this, we reach the much more significant conclusion that electron transfer rates involving oxo-bridged dimers appear to be substantially slower than that of the hydroxo-bridged dimers since $k_{obs}^{(hydroxo)} > k_{obs}^{(oxo)}$. Thus, the data in Figure 4, while

(70) Bock, C. R.; Connor, J. A.; Gutierrez, A. R.; Meyer, T. J.; Whitten, D. G.; Sullivan, B. P.; Nagle, J. K. *J. Am. Chem. Soc.* **1979**, *101*, 4815.

(71) This analysis does not apply for data on the hydroxo-bridged quenchers since these reactions are diffusion-limited.

demonstrating a significant difference in rates of quenching, actually imply a much more pronounced difference in electron transfer reactivity between the two classes of compounds.

Assessing whether Dexter transfer is operative at all in these systems is difficult. There is ample precedent in the literature to indicate that, when both electron and Dexter energy transfer pathways are available, the electron transfer route is generally preferred. This is due to the double exchange nature of Dexter transfer and the corresponding reduction in the rate by a factor of e^2 which manifests in the electronic coupling term. However, in favorable circumstances this can be offset by a sufficiently large change in the barrier associated with the reaction such that the exponential term in the Franck−Condon factor dominates. We have already indicated that we do not expect significant changes in the reorganization energy for electron transfer in oxo- versus hydroxo-bridged reactions, but changes in reorganization energy following energy transfer are more difficult to estimate. Given that both classes of compounds have closely related electronic structures, it is not immediately obvious why the oxo- and hydroxo-bridged complexes should be significantly different in their structural response to either ligand-field or charge transfer excitation. These considerations, coupled with the conclusions inferred from the slope of the data in Figure 4, point to changes in electron transfer rates as being the dominant factor defining differences in reactivity between these systems. Still, additional work is clearly needed in order to examine the issue of energy transfer more thoroughly. The specific role of electronic coupling between the donors and acceptors (for both energy and electron transfer) is likewise unclear at this point. In an absolute sense it is an extremely important parameter, but estimating what differences may exist in this term for the oxo- and hydroxo-bridged systems upon collision with the sensitizer in solution would be pure speculation. This represents an intrinsic limitation with the present study that must be overcome in future work.

Concluding Comments

From an experimental perspective, the convolution of quenching mechanisms, Heisenberg exchange, driving force, reorganization energy, and electronic coupling presents a very complex problem for understanding the effects of spin exchange on chemical reactivity. While the work presented herein does not provide a definitive resolution, we believe that several important steps have been taken as a result of this study:

1. It was demonstrated that exchange-coupled dinuclear Fe^{III} complexes can act as electron acceptors following photoexcitation of an appropriate donor.

2. The driving force for electron transfer to oxo/hydroxo-biscarboxylato dinuclear Fe^{III} complexes can be cleanly decoupled from changes in Heisenberg exchange by simply changing the identity of the bridging carboxylate.

3. When a series of complexes are prepared according to the guidelines indicated in step 2, a dependence of quenching on ΔG_0^{ET} is observed. However, changes in driving force are not sufficient to explain reactivity differences between oxo- and hydroxo-bridged Fe^{III} dimers.

4. Structural variations in the dinuclear Fe^{III} systems are relatively insensitive to changes in the identity of the bridging carboxylate. Furthermore, the anticipated changes in both inner-sphere and outer-sphere reorganization energies following reduction of the clusters to the $Fe^{II}Fe^{III}$ mixed-valent state are expected to be approximately equal for both the oxo- and hydroxo-bridged complexes.

5. Combining all of the data, the conclusion is reached that reactivity differences between oxo- and hydroxo-bridged dinuclear Fe^{III} complexes must be due to accelerated rates of Dexter and/or electron transfer to the hydroxo-bridged complexes. Data analysis suggests that significant differences in electron transfer rates are in evidence; furthermore, it is clearly established that modulation of reactivity is not linked in any straightforward way to either the driving force or reorganization energy for electron transfer.

It is of course tempting to point to Heisenberg exchange as an important factor in defining and differentiating the chemistry exhibited by these systems. Theoretically, as stated by Bersuker et al.,[13] changes in the transmission frequency for electron transfer can be modulated by spin exchange within a molecule. The data we have presented clearly agree with the central premise of this model. However, we believe that a direct experimental link between spin exchange and reactivity is still premature at this stage. Limitations endemic to the study of bimolecular quenching reactions including diffusion as well as uncertainty in the relative magnitudes of the electronic matrix elements governing donor/acceptor coupling prevent us from drawing such definite conclusions. It is therefore our considered opinion that the study we have presented here approaches the limit to which the interrelationship between Heisenberg exchange and electron/energy transfer dynamics can be addressed in the context of a bimolecular reaction. However, most if not all of the problems that have been alluded to can be overcome if the chemistry is studied as an intramolecular process. Work along these lines is currently in progress.

Acknowledgment. The authors thank Professors Harry Gray, Morton Hoffman, Daniel Nocera, and Dr. Catherine Clark for helpful discussions, and Professor Angelica Stacy for use of the SQUID magnetometer. This work was supported through funds from the National Institutes of Health, National Institute for General Medical Sciences (Grant GM58551-02), the Hellman Foundation, and the Alfred P. Sloan Foundation (J.K.M.).

Supporting Information Available: Complete tables of crystallographic data, positional parameters, equivalent isotropic thermal parameters, bond distances, bond angles, and anisotropic thermal parameters. This material is available free of charge via the Internet at http://pubs.acs.org.

IC010659L